Supporting Information

Copper Core - Porous Manganese Oxide Shell Nanoparticles

Nachal D. Subramanian[1], Juana Moreno[2], James J. Spivey[1] and *Challa S.S.R. Kumar[3]**

[1]Cain Department of Chemical Engineering, Louisiana State University, Baton Rouge, LA 70803 (USA)
[2]Department of Physics & Astronomy and Center for Computation & Technology, Louisiana State University, Baton Rouge, LA 70803 (USA)
[3]Center for Advanced Microstructures and Devices, Louisiana State University, Baton Rouge, LA 70806 (USA)
Corresponding author email: ckumar1@lsu.edu

Experimental

Materials Characterization

In order to characterize the size distribution of the $Cu@Mn_3O_4$ nanoparticles, small angle X-ray scattering (SAXS) experiments were carried out using the SAXS beamline at LSU/CAMD. A double-crystal monochromator allows photons with energy range from ~3-14 KeV. SAXS pattern is imaged with 200 mm x 200 mm multiwire gas detector with a resolution of 200-250 μm FWHM in a 1024 x 1024 array. A segmented flight path allows q-range from 0.0015 to 0.44 Å^{-1} to be studied. Dilute toluene solutions of dispersed nanoparticles were filled into 1 mm quartz capillary tubes in inert atmosphere and sealed.

X-ray diffraction (XRD) patterns were recorded on a Bruker/Siemens D5000 automated powder X-ray diffractometer, using Cu Kα radiation (λ = 1.540562 Å) with Rietveld analysis

software. X-ray photoelectron spectroscopy (XPS) studies were performed on a Kratos AXIS 165 X-ray Photoelectron Spectroscope and Scanning Auger Microscope equipped with standard Mg/Al source and high performance Al monochromatic source. Fourier transform infrared spectroscopy (FTIR) spectra were obtained using a Thermo Nicolet 6700 spectrometer equipped with a MCT detector. A diamond crystal attenuated total reflectance (ATR) accessory was used for measurements. Spectra were collected at 4 cm^{-1} resolution and 32 scans.

Results and Discussion

(a) XPS

The Cu/Mn surface atomic ratios as well as the binding energies of the main peaks were obtained by XPS measurements for the $Cu@Mn_3O_4$ nanoparticles (Table S1). The results indicate that the surface Cu/Mn ratio is 2.2:1, indicating a surface enrichment of copper. This could be due to either the presence of Cu oxide in the shell or the Cu-core being accessible through the porous shell. The Cu $2p_{3/2}$ peak at 932.6 eV corresponds to Cu^0 and/or Cu_2O, but the XPS spectrum did not reveal any shake up satellites corresponding to Cu_2O. Also, the difference in the $2p_{3/2}$ and $2p_{1/2}$ energies is about 19.9 eV, corresponding to metallic copper [1]. However, although it is most probable the presence of metallic copper, there is also the possibility of the copper core getting partially oxidized during sample loading since the shell is porous. The Mn $2p_{3/2}$ peak is positioned at 641.7 eV and the difference between the binding energy values of Mn $2p_{3/2}$ and Mn $2p_{1/2}$ level is 11.9 eV, which matches values for many types of manganese oxides. Therefore, the discrimination becomes very difficult and a definite conclusion about the oxidation state of Mn cannot be derived from the XPS results.

Table S1. XPS analysis of Cu@Mn$_3$O$_4$ nanoparticles.

Binding energies (eV)		Cu/Mn surface atomic ratio	Oxidation states
Cu 2p$_{3/2}$	Mn 2p$_{3/2}$		
932.6	641.7	2.2	Cu^0 and/or Cu$_2$O Mn^{2+} and/or Mn^{3+}

(b) SAXS

Figure S1 shows the SAXS data for pure copper and Cu@Mn$_3$O$_4$ nanoparticles. SAXS data represent the scattering cross section per unit sample volume, I(Q), as a function of scattering vector Q. Figure S1 also displays the particle size distribution derived from the SAXS data assuming the spheroid particle model and a non-negative least squares (NNLS) fitting method. A unimodal size distribution is observed in both systems. The approximate average particle size of Cu nanoparticles (Figure S1a) is around 7-12 nm, while the Cu@Mn$_3$O$_4$ nanoparticles (Figure S1b) have a very narrow unimodal size distribution of around 17-20 nm. The symmetrical size distribution indicates the absence of any particle agglomeration, and the average particle size of the nanoparticles is found to increase with the shell coating. However, the particle sizes obtained from SAXS fits are slightly larger than those obtained from the TEM. This difference could be attributed to the fact that SAXS information is generated from a large sampling volume and hence a larger number of particles are probed compared to TEM. Also, the fitting method and the particle model assumed for fitting the data could have led to some disparities.
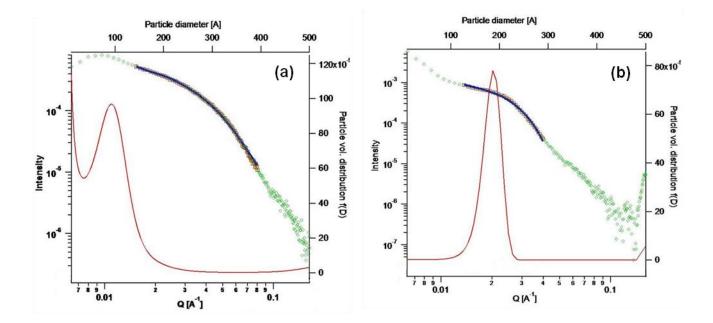
Figure S1. SAXS data and particle size distribution derived using the spheroid particle model and the NNLS fitting method for (a) Cu nanoparticles and (b) Cu@Mn$_3$O$_4$ nanoparticles.

(c) FTIR

In order to confirm the adsorption of surfactants used during synthesis – oleic acid (OA) and trioctylphosphine (TOP), FTIR spectra of the as-prepared Cu@Mn$_3$O$_4$ nanoparticles was recorded. The resulting infrared spectra in the 700-3200 cm^{-1} region is shown in Figure S2. It has been reported that oleic acid binds to nanoparticle surfaces through the –COO$^-$ group in both monodentate and bidentate forms [2-3] and TOP binds via C-P modes. From Figure S3, **t**he peaks at 2847 and 2916 cm^{-1} can be assigned to the symmetric & asymmetric CH$_2$ stretching modes and the peak at 3001 cm^{-1} is due to the v(C-H) mode of the C-H bond adjacent to the C=C bond. All these bands in the region 2850-3000 cm^{-1} are characteristic of both OA and TOP surfactants.

4

The bands at 1530 and 1395 cm^{-1} can be attributed to the symmetric and asymmetric vibrations of the $-COO^-$ group of oleic acid, indicating the presence of bidentate carboxylate bonding to the nanoparticles. However, the v(C=O) stretching mode of the carboxylic acid group found in pure oleic acid [2], was present only as a small broad shoulder at 1709 cm^{-1}, and a decrease of the intensity of this band after surfactant binding on the nanoparticles is indicative of the chemical adsorption of oleic acid to the surface of the nanoparticles. Sharma et al. attributed the absence of this peak on oleic acid stabilized CoNi nanoparticles to a similar assignment [3]. Peaks in the low frequency region (< 1500 cm^{-1}) arise from complex combinations of C-C and C-O stretches, CH_2 deformations, etc [2]. The peaks in the range 1000-1170 cm^{-1} are due to the C–P stretching modes of TOP [4]. Also, the shoulders at 1462, 1456 and 1377 cm^{-1} are reported to originate from the terminal methyl groups of TOP [4]. Overall, the bands arising specifically due to TOP adsorption are relatively lower in intensity compared to those due to oleic acid. This might indicate that the metal-TOP complexes decompose at the synthesis temperature (200 °C) whereas oleic acid strongly chemisorbs on the nanoparticle surface. All the bands observed in the FTIR spectra point toward the existence of organic ligands from surfactants that are capped onto the nanoparticle surface, thereby preventing further agglomeration of the particles. This was also further confirmed by the detection of CO_2, CH_4 and H_2O as products when the nanoparticles were oxidized under 10% O_2/He.
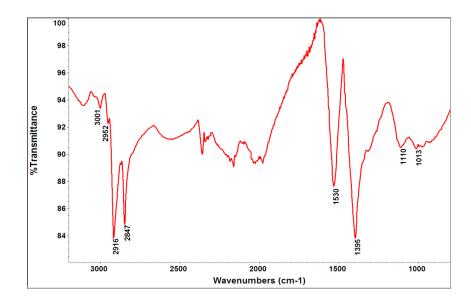
Figure S2. FTIR spectrum of Cu@Mn$_3$O$_4$ nanoparticles in the 800-3200 cm^{-1} region.

(e) XRD

The major peaks in the XRD pattern (Figure S3) can be identified as face-centered cubic Cu. XRD peaks are observed at 2θ values of around 43.4°, 50° and 74°, which are in a good agreement with the standard XRD pattern of metallic Cu [5], consistent with the XPS assignments. The diffraction peaks at 2θ = 29.3°, 36.5°, 61°, 74° can be attributed to Mn$_3$O$_4$ [6-9].
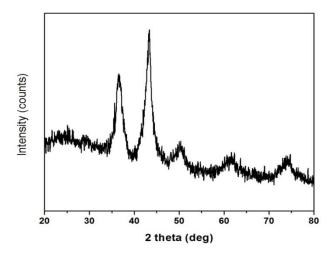

Figure S3. X-ray diffraction pattern of Cu@Mn$_3$O$_4$ nanoparticles.

References

1. Frost, D. C.; Ishitani, A.; McDowell, C. A. *Mol. Phys.* **1972**, *24 (4)*, 861-877.

2. Shukla, N.; Liu, C.; Jones, P. M.; Weller, D. *J. Magn. Magn. Mater.* **2003**, *266*, 178-184.

3. Sharma, S.; Gajbhiye, N. S.; Ningthoujam, R. S. *J. Colloid Interface Sci.* **2010**, *351 (2)*, 323-329.

4. Chen, S. T.; Zhang, X. L.; Zhang, Q. H.; Tan, W. H. *Nanoscale Res. Lett.* **2009**, *4 (10)*, 1159-1165.

5. Singh, M.; Sinha, I.; Premkumar, M.; Singh, A. K.; Mandal, R. K. *Colloids Surf., A* **2010**, *359 (1-3)*, 88-94.

6. Chang, Y. Q.; Xu, X. Y.; Luo, X. H.; Chen, C. P.; Yu, D. P. *J. Cryst. Growth* **2004**, *264 (1-3)*, 232-236.

7. Al Sagheer, F. A.; Hasan, M. A.; Pasupulety, L.; Zaki, M. I. *J. Mater. Sci. Lett.* **1999**, *18 (3)*, 209-211.

8. Park, J.; Kang, E. A.; Bae, C. J.; Park, J. G.; Noh, H. J.; Kim, J. Y.; Park, J. H.; Hyeon, T. *J. Phys. Chem. B* **2004**, *108 (36)*, 13594-13598.

9. Xu, H. Y.; Xu, S. L.; Wang, H.; Yan, H. *J. Electrochem. Soc.* **2005**, *152 (12)*, C803-C807.